We are IntechOpen,
the world's leading publisher of
Open Access books
Built by scientists, for scientists

7,000
Open access books available

187,000
International authors and editors

205M
Downloads

154
Countries delivered to

Our authors are among the

TOP 1%
most cited scientists

12.2%
Contributors from top 500 universities

WEB OF SCIENCE™

Selection of our books indexed in the Book Citation Index
in Web of Science™ Core Collection (BKCI)

Interested in publishing with us?
Contact book.department@intechopen.com

Numbers displayed above are based on latest data collected.
For more information visit www.intechopen.com

Nanoparticles and Nanostructures for Biophotonic Applications

Enzo Di Fabrizio[1,2] et al.[*]
[1]Nanostructures Department, Italian Institute of Technology, Genova,
[2]BioNEM lab., Departement of Clinical and Experimental Medicine,
Magna Graecia University, Viale Europa, Catanzaro,
Italy

1. Introduction

The aim of this chapter is to expound on the theoretical analysis and experimental assessment of NanoParticles (NPs) for imaging, early detection and therapeutic applications. NPs are extremely small particulates with dimensions ranging from few micrometers down to few tens of nanometers. Their characteristics, including size, shape, physical and chemical properties, can be tailored during the fabrication/synthesis process and, on account of these, they would feature certain aspects that may be exploited for applications ranging from drug delivery to the enhancement of the local electric field, and thus the detection of few molecules. In particular, intravascularly injectable NPs (that are sometimes called nanovectors or nanocarriers) are probably the major class of nanotechnological devices of interest for use in cancer or, in general, for the treatment of diseases. On the other hand, aggregates of metallic NPs, either of silver or gold, represent extremely efficient SERS (Surface Enhanced Raman Scattering) substrates. In the following, after a brief description of NPs as a whole, a number of different applications will be discussed.

2. Nanoporous silicon nanoparticles: A drug delivery system

Intravascularly injectable NPs can be conveniently designed or engineered to release drug molecules or imaging tracers with a superior performance with respect to freely administrated agents (Ferrari, 2005; Whitesides, 2003; La Van et al., 2003); to this extent, they represent smart Drug Delivery Systems (DDS).

[*] Francesco Gentile[1,2], Michela Perrone Donnorso[1,3], Manohar Chirumamilla Chowdary[1],
Ermanno Miele[1], Maria Laura Coluccio[1,2], Rosanna La Rocca[1], Rosaria Brescia[4], Roman Krahne[1],
Gobind Das[1], Francesco De Angelis[1], Carlo Liberale[1], Andrea Toma[1], Luca Razzari[1],
Liberato Manna[4] and Remo Proietti Zaccaria[1]
[1]Nanostructures Department, Italian Institute of Technology, Genova, Italy
[2]BioNEM lab., Department of Clinical and Experimental Medicine, Magna Graecia University, Viale Europa, Catanzaro, Italy
[3]Nanophysics Department, Italian Institute of Technology, Genova, Italy
[4]Nanochemistry Department, Italian Institute of Technology, Genova, Italy
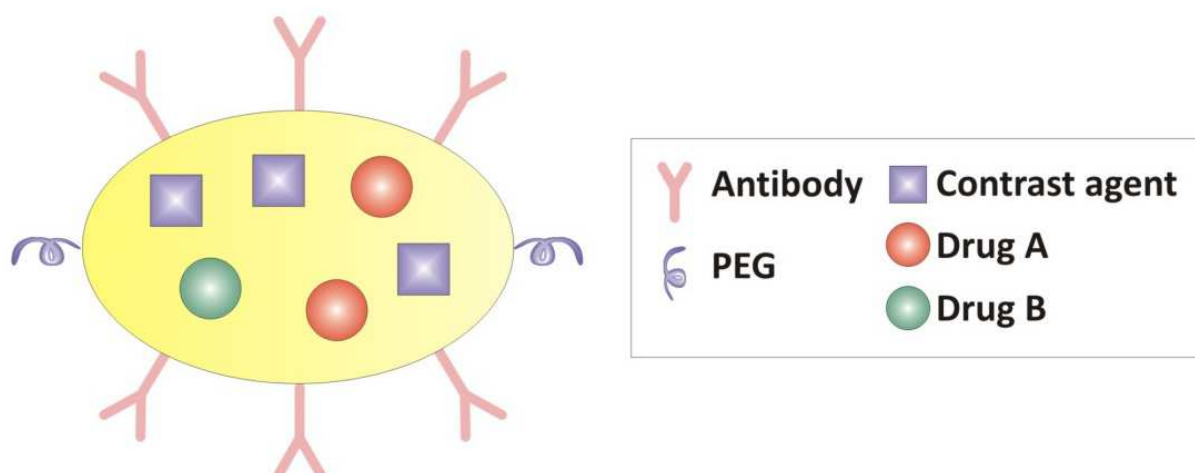
Fig. 1. Cartoon representing a nanoparticle featuring different coverings and payloads.

In other terms, on account on their geometrical, physical and chemical properties (**Fig.1**), the therapeutic or contrast agents would be targeted directly towards the site of interest (malignant cells) with a significant reduction of side effects, and a concurrent increase in the efficiency of delivery.

Liposomes are the simplest form of NPs (and, accordingly, they are sometimes referred to as first generation nanovectors) (Klibanov et al., 1991; Park, 2002; Crommelin & Schreier, 1994). Established for the treatment of Kaposi's sarcoma more than 10 years ago, nowadays certain liposomes based NPs are still being used for cancer treatment. Literature records a massive number of second generation NPs, (which, differently from liposomes, can be artificially produced using nanofabrication techniques), including polymer-based nanovectors, silicon and silica NPs and metal-based nanovectors like nanoshells (Kircher et al., 2003; Schellenberger et al., 2002; Zhang & Shang, 2004; Cohen et al., 2003; Hirsch et al., 2003; Langer, 1998; Duncan, 2003; Gilles & Frechet, 2002).

Despite this, and notwithstanding the merits that such an abundance of devices provides in terms of novel technological foundations and opportunities, only a small amount of these nanovectors would be really effective in delivering drugs or contrast agents (Ferrari, 2005).

A number of third generation NPs is currently under development which feature advanced properties and thus more efficacious delivery modalities, including nanoporous NPs with/without reduced silver for SERS analysis, mesoporous silicon particles as a multistage delivery systems, nanoporous NPs enhancing, via geometrical confinement of gadolinium-based contrast agents, T_1 contrast (Tasciotti et al., 2008; Jeyarama et al., 2010).

In general, an ideal nanoparticle should be able (i) to navigate into the circulatory system avoiding the immune system and recognizing the diseased cells (biological target) with high selectivity; (ii) to adhere firmly to them and (iii) to allow for endocytosis process. Targeting methods have been largely investigated and range from specific (covalently linked ligands decorate nanovectors and may recognize antibodies over-expressed on the cells of interest) to non specific (that are, mechanisms based on the size, shape and physical properties of the nanovector including density, porosity, surface charge) (Decuzzi, 2006a, 2006b, 2007).

Regardless the particular mechanisms of transport and adhesion that NPs can experience, it is clear that a thorough understanding of the physics behind these phenomena plays a fundamental role. Realistically, mathematical models provide an unprecedented tool for predicting the behaviour of NPs within the macro/microcirculation, thus also supplying a rationale for the best design of NPs (Gentile, 2007, 2008). In DDS the choice of bulk material constituent the nanocarrier is a key point since it must fulfill a tailored biological behavior (bioactivity, biocompatibility, biodegradability), it must improve payload capacity and be harmlessly eliminated from the body in a reasonable period of time after releasing the cargo and having carried out possible diagnostic function (Park et al., 2009). While many proposed nanocarriers do not meet these requirements, porous silicon (PSi), considered as silicon crystal having a series of voids, is a promising materials for its biocompatibility and biodegradability (Granitzer & Rumpf, 2010; Canham, 1997; O Farrel et al., 2006) which results in decomposition products not harmful for biological system. Porous silicon dissolves in body fluids into orthosilicic acid, commonly found in everyday foods and efficiently excreted from the body through the urine (Park et al., 2009). Thanks to the porous structures, silicon nanoporous nanoparticles show a great surface/volume ratio (200-800 m^2/cm^3) (Halimaoui, 1995), a very attractive characteristic since surface can be used to load drugs by physisoprtion process and modified with molecules that promote cell adhesion. Pore width, porosity and nanoparticles size can be tuned by adjustment of the parameters during the fabrication process. When the pore size is in the range of 2-5 nm, physisorbed drugs are efficiently entrapped and, due to the effect of the quantum confinement of the silicon structure (Godefroo et al., 2008), particles show emission at 620 nm (red-orange) at room temperature under UV illumination (wavelength of 365 nm), a very attractive feature for the realization of theranostic nanoparticles (Janib, 2010). Pores population can be divided in two different types: open pores that are connected to each other and to the external surface and closed pores isolated from the outside, that are less useful for drug delivery purpose.

Porosity is defined as the fraction of void in the porous structure. High porosity means great surface/volume ratio and it is preferable for drug delivery device, however, due to the surface tension, too high porosity silicon layer can undergo to collapse during the fabrication process and the obtained nanoparticles can disintegrate in water solution. Size and shape are two important features of nanoparticles used in drug delivery systems. Nanoporous silicon nanoparticles with size of 30-100 nm are suitable carriers for many anticancer agents (Petros & DeSimone, 2010; Mitragotri & Lahan, 2009).

2.1 Fabrication and characterization of NanoPorous Silicon Particles

The most widely used method to fabricate Nanoporous Silicon Nanoparticles (NPNPs) is a process that includes several steps, starting from the production of nanoporous silicon film by an electrochemical etching in ethanol/HF solution of Si wafer, in which silicon acts as an anode and a platinum electrode acts as a cathode. Since Si wafer surface is hydrophobic, ethanol increases the wettability of the substrate allowing the electrolyte penetrating into the pores and also helps in removing the H_2 bubble from the sample surface formed during the anodization process (Canham, 1997). A constant current density is applied to allow the formation of homogeneous porous layer. Samples are rinsed in de-ionized water, then in ethanol and pentane, and sonicated in water for a time

required to remove all the nanoporous silicon film from the crystalline silicon substrate. The film is then fractured by ultrasonication and filtered through filtration membrane and centrifuged in order to select the desired particles size. It is possible to vary NPNPs morphology (pore size and distribution, pores interconnectivity, porosity and particles diameter) changing the fabrication parameters such as etching time, anodization current density, HF concentration, wafer type and ultrasonication time. Tab.1 shows the effect of some fabrication parameters on the formation of NPNPs as produced by the authors. Freshly anodized PSi has a remarkable surface hydrophobicity (contact angle ~110°, depending on porosity and surface roughness), a very attractive property that could be used in biomedical field to design nanostructure that enable plasma protein harvesting and concentration (Pujia et al., 2010). However hydrophobicity is a limitation in case of hydrophilic drugs loading, in this case porous silicon hydrophobic behavior has to be changed in hydrophilic one by thermal treatment just before porous silicon film sonication. To prevent particles aggregation and dissolution fabricated NPNPs are stored at 4°C until using.

Sample	Etching conditions (HF 25%/ethanol 1:2 v/v)	Ultrasonication time	Particles Size	Pore size	Gravimetric Porosity
p-type	J =10 mA/cm^2 for 300 sec	10 min	101± 34 nm	< 20 nm	80%
p-type	J =10 mA/cm^2 for 720 sec	10 min	75 ±24nm	< 10 nm	87%
p-type	J =10 mA/cm^2 for 720 sec	20 min	30 ±15nm	< 10 nm	87%
p++	J =10 mA/cm^2 for 720 sec	10 min	65±24 nm	< 5 nm	65%

Table 1. Characterization of p-type silicon nanoparticles varying the fabrication parameters.

The porosity of the porous silicon layer, is determined by gravimetric measurements, weighing the silicon substrate both before and after anodization (m1 and m2 respectively) and again after the complete dissolution of the porous layer by 25% KOH solution (m3). Porosity(P) is calculated by the relation P = (m1-m2)/(m1-m3). Particles Dynamic Light Scattering (DLS), Transmission Electron Microscopy (TEM) and Scanning TEM (STEM) analyses are commonly used to determine hydrodynamic size and pores width of NPNPs. Porous silicon nanoparticles can be investigated using BET – BJH theory as well. BET (Brunauer – Emmet – Teller) adsorption isotherms allow for the calculation of surface / volume ratio (m^2/cm^3) and Barrett-Joyner-Halenda (BJH) method can be used in pores width (nm) and volume (cm^3/g) determination. **Fig.2** shows TEM, STEM and DLS analysis of nanoparticles as developed in the authors' laboratory. Nanoparticles chemical analysis, performed by X-ray energy dispersive spectroscopy (EDS), indicates that fluoride is a common contaminant that is residual from the electrolyte solution used during the fabrication and disappears during annealing at 300°C as shown in **Fig.3**.
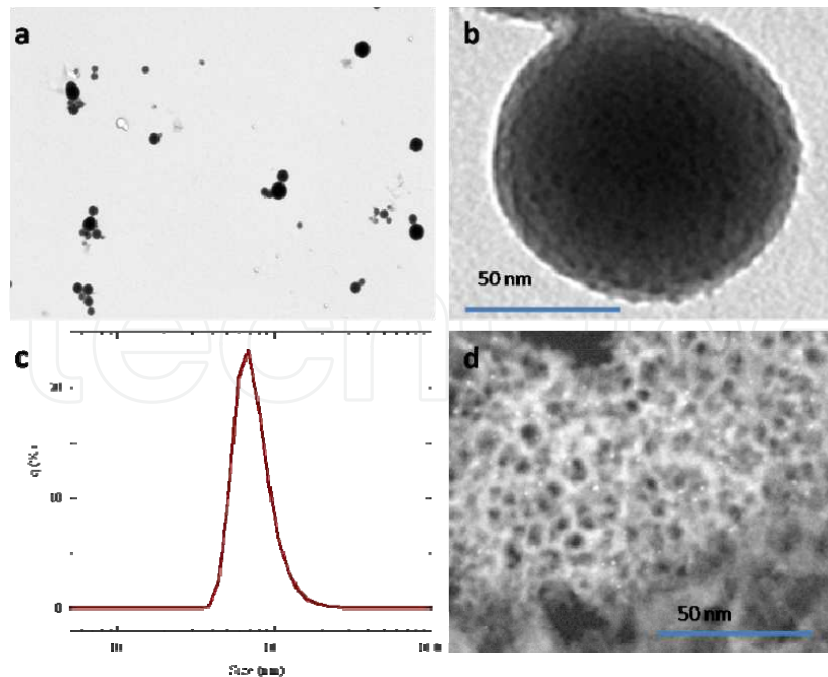
Fig. 2. TEM images (a, b), DLS size distribution (c) and STEM–HAADF image (d) of 75 nm porous silicon nanoparticles
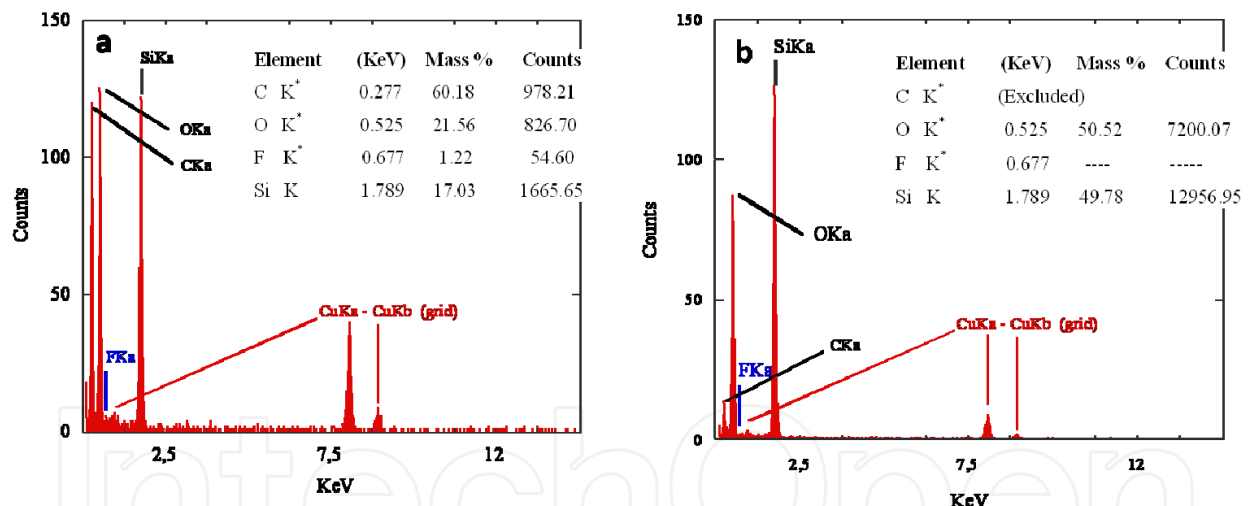

Fig. 3. Chemical analysis with EDS of nanoporous silicon NPs before (a) and after (b) annealing at 300°C.

In order to evaluate the cytotoxicity of NPNPs, apoptosis test has been performed by using iodure propidium agent and cytofluorimetric analysis. Human colon carcinoma cells (HCT116) and health monocytes (THP1) were incubated with 100 µg of two different types of NPNPs (before and after annealing) for 48 h in RPMI 1640 medium at 37°C at 5% CO_2 and cell viability detected and compared with control samples treated with medium only (**Fig.4**). No significant toxic effect was observed in the two cell lines incubated with NPNPs compared with controls. In order to evaluate the really usefulness for therapeutic applications, drug loading can be carried out by physisorption process, incubating NPNPs with drug in water at room temperature overnight. Loaded nanoparticles can be recovered

from the solution by centrifugation at 12,000 rpm for 30 minutes. The amount of incorporated drug can be quantified through UV-Visible spectroscopy analysis of supernatant compared with drug standard curve. In the case of anti cancer Doxorubicin, loading test performed in the authors' laboratory, shows 5% (weight) payload for NPNPs obtained from silicon film annealed at 260°C for 4h, while a stronger thermal treatment (500°C for 12 h) can enhance physisorption process. Drug embedded NPNPs could be stored in DI water at 4°C for long time while under physiological conditions dissolve in 120 hours releasing the loaded drug (Pujia et al., 2010; De Angelis, 2010a).
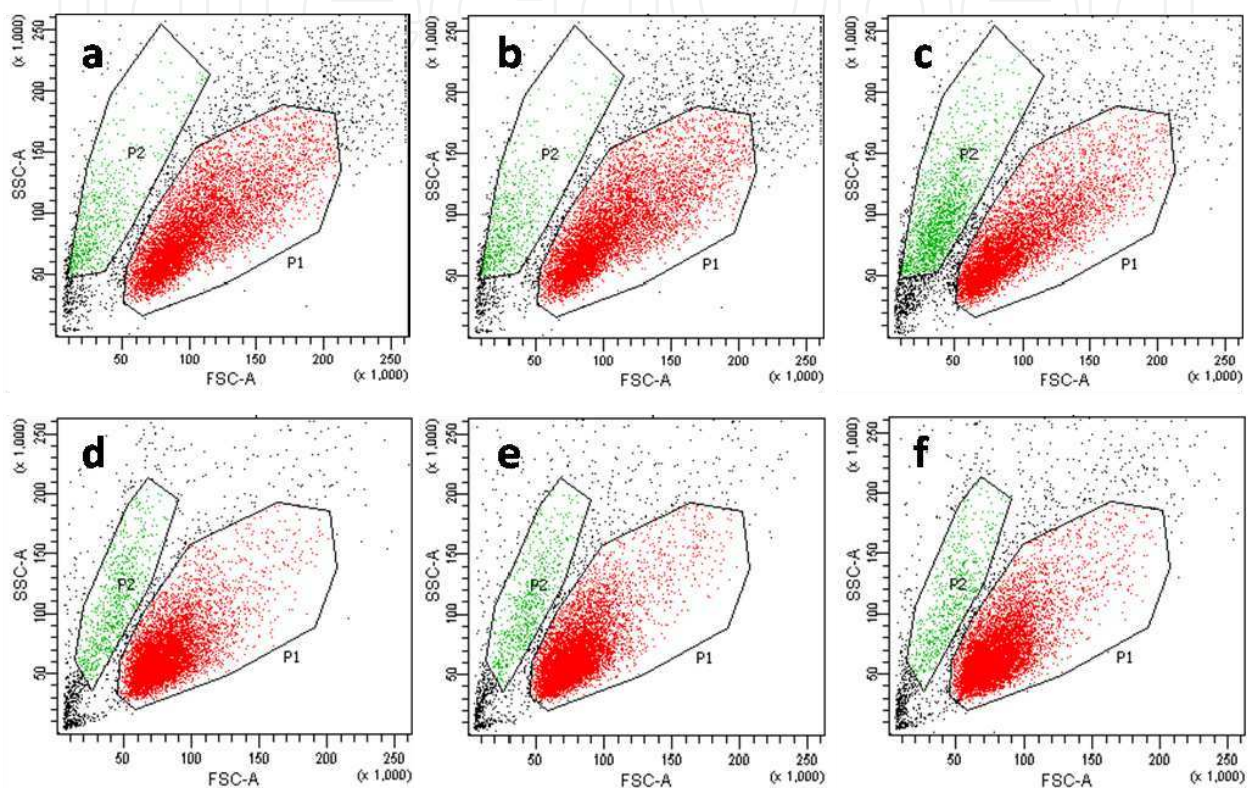

Fig. 4. Density plot of HCT116 (a, b, c) and THP1 (d, e, f) cell lines. Gate P1 shows cell viability %. a) HCT116 cells control without NPNPs, (P1 79%). b) HCT116 cells incubated with not annealed NPNPs (P1 78%). c) HCT116 cells incubated with annealed NPNPs (P1 68%). d) THP1 cells control without NPNPs (P1 83%). e) THP1 cells incubated with not annealed NPNPs (P1 82%). f) THP1 cells incubated with annealed NPNPs (P1 82%).

In conclusion, porous silicon nanoparticles represent a powerful and versatile tool in developing new drug delivery strategies, with high loading capacity, biocompatibility, cheap and scalable fabrication process. Porous silicon-based nanocarriers properties (size, shape and surface chemistry) can be easily tuned operating on the fabrication parameters to achieve a tailored biological behavior and improved bioavailability of transported drug.

3. Core-shell nanorods for light emitting applications

Inorganic semiconductor nanocrystals hold a great promise for emerging nanotechnologies, since they feature physical and chemical properties unique to the

nanometer length scale, which are useful for diverse applications such as microelectronic and optical devices, as well as for sensing. These properties depend not only on the nanoparticle's composition, but also on its *size*, *shape*, and *mode of organization*. For this reason, a major effort has been dedicated in recent years to the development of synthetic methods providing control over morphological parameters of the nanocrystals and their assembly into organized structures. Colloidal synthesis, where judicious choice of protective ligands is employed to morphologically control crystal growth, has proven to be the most versatile approach for the synthesis of non-spherical nanoparticles, providing a variety of shapes, such as rods, prisms, cubes, disks, and others. In this section we will focus on *rod-shaped* nanocrystals, whose shape anisotropy is translated into polarized physical properties (Hu et al., 2001), and which can be harnessed for the creation of polarized light emitting materials (Kazes et al., 2002, 2004; Rizzo et al., 2009). For an extensive review on the physical properties of rod-shaped nanocrystals we refer the reader to reference (Krahne et al., 2011a). In particular, we will discuss a novel core-shell architecture for nanorods, in which a spherical core of a smaller band gap material is embedded in a rod-shaped shell of a high band gap semiconductor (Talapin et al., 2003; Carbone et al., 2007) as sketched in **Fig.5a**.
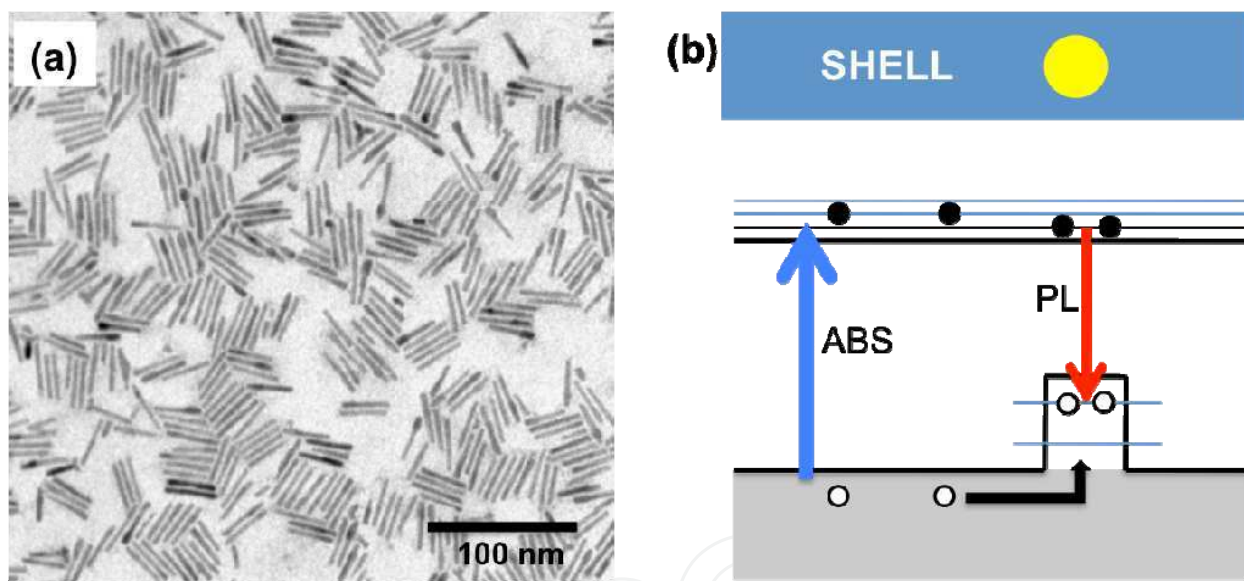

Fig. 5. (a) Transmission electron microscopy image of core shell nanorods. Scheme of the CdSe/CdS core-shell nanorod architecture and of the related band structure.

Such a system is often referred as "dot-in-a-rod", where the charge carriers can be excited in the UV-blue spectral region and then quickly (on the picosecond timescale) relax into the more long living core states from which the light emission occurs (Lupo et al., 2008). The core-shell nanorods have numerous advantages concerning their optical emission properties: (i) the stronger confinement in the core leads well defined energy levels for the optical transitions. (ii) The shell passivates the surface states of the emitting low band gap material. (iii) Due to their rod shape they have an enhanced absorption cross section with respect to spherical particles. In the specific case of CdSe/CdS core shell nanorods the lower energy levels of the holes are localized in the core, whereas the electrons are mostly delocalized over the rod volume, as illustrated in **Fig.5**. This particular electronic level

structure proved to reduce non-radiative Auger recombination significantly (Zavelani-Rossi, 2010a) and therefore provides great advantages for lasing devices. Furthermore, the energy of the emitting light is determined by the quantum confinement in the core, which allows to tune their emission wavelength independently of the rod length, at least to a certain extent (Krahne, 2011b), as can be seen in **Fig.6**, which shows emission spectra of core shell nanorods with different core diameter and rod length.
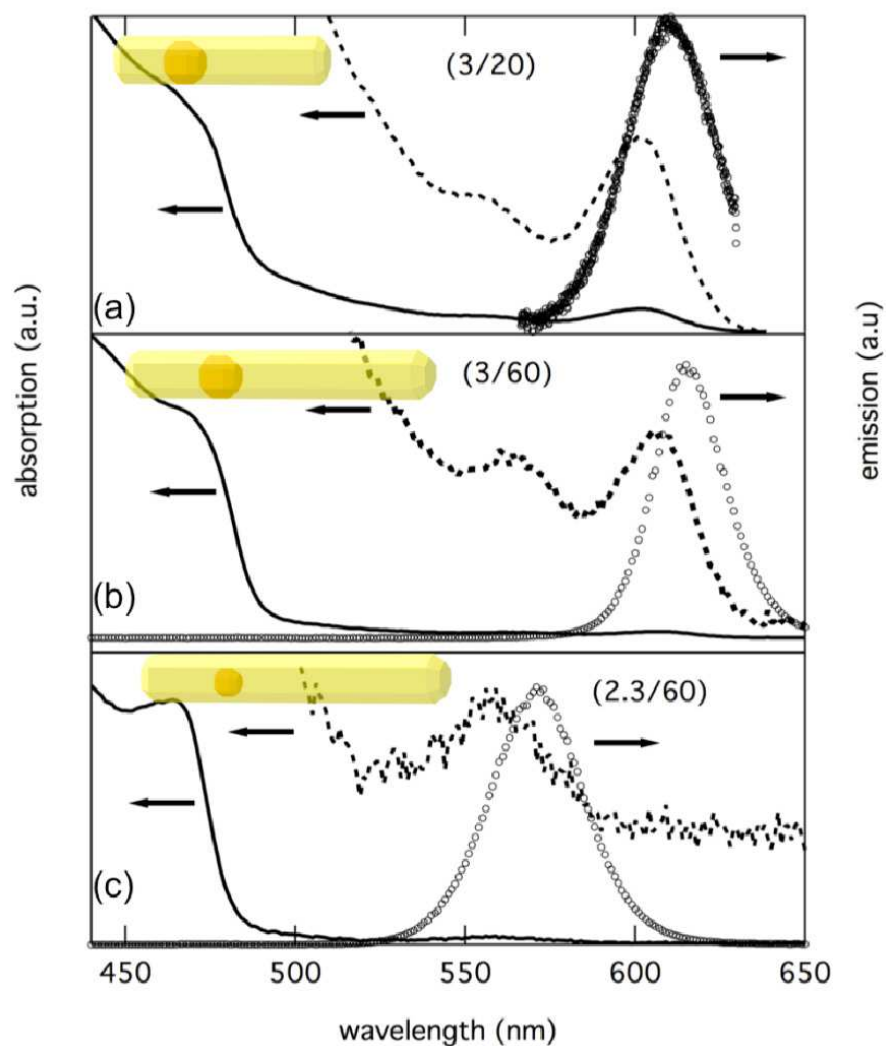

Fig. 6. Absorption and emission spectra of core-shell CdSe/CdS nanorods with different core sizes and different lengths. The core diameter and the rod length are specified by the numbers in brackets in units of nm. The emission wavelength is dominated by the core size. Taken with permission from (Krhane et al., 2011a).

Light emission from the nanorods can be obtained either by optical or via electrical pumping. In the latter case the charge carriers are injected via external electrodes that are in contact with the nanorods. Metal electrodes have the disadvantage that a Schottky barrier is formed at the interface with semiconductor material which significantly hinders

the charge injection. Furthermore, the nanorod luminescence gets quenched by a direct contact of the nanorods with a metal, for example with gold. Instead, the implementation of a nanorod layer in a sandwich-like geometry, in between hole- and electron-injection organic layers, has proven to be a successful approach to fabricate light emitting diodes (LED) based on semiconductor nanorods as the active material (Rizzo et al., 2009). **Fig.7** illustrates this fabrication scheme where an ITO (indium-tin-oxide) substrate is used as a back electrode onto which *a N,N*=-bis(naphthalen-1-yl)-*N,N*=-bis(phenyl)benzidine (-NPD) hole injection layer (HIL) doped with 2,3,5,6-tetrafluoro-7,7,8,8-tetracyanoquinodimethane (F4-TCNQ) and a CBP hole transporting layer (HTL) were thermally evaporated
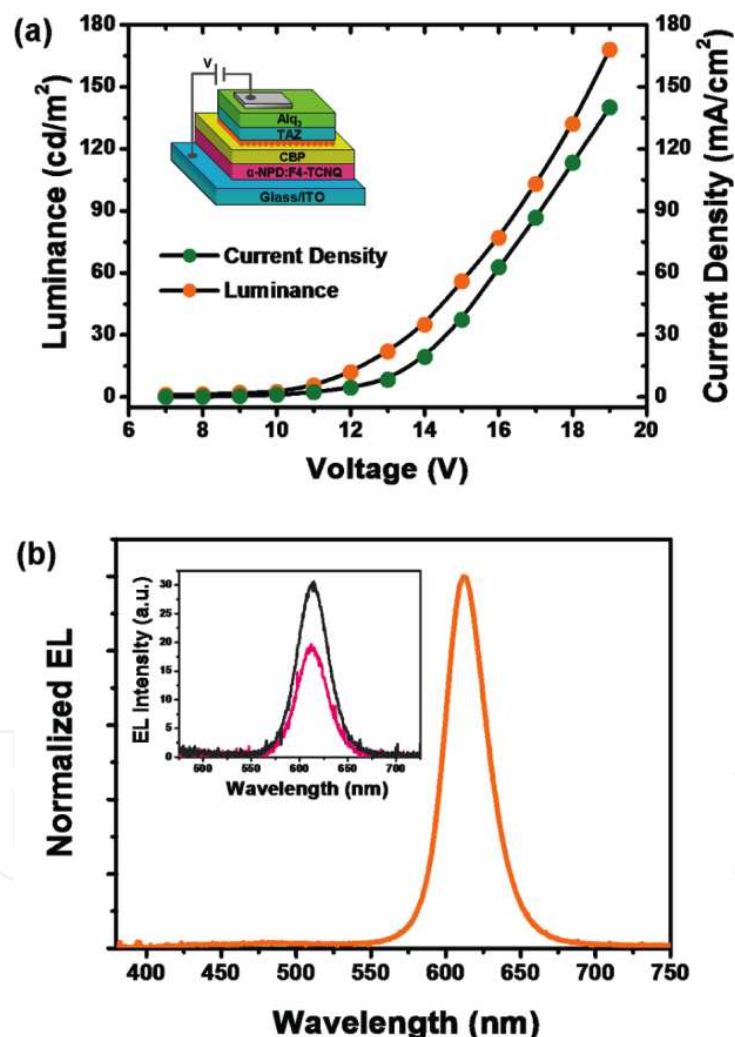

Fig. 7. (a) Current density and luminance from a LED based on an oriented layer of laterally aligned core-shell nanorods as illustrated by the scheme in the inset.
(b) Electroluminescence spectrum. The inset shows two spectra for orthogonal polarization directions. Taken with permission from (Rizzo et al., 2009).
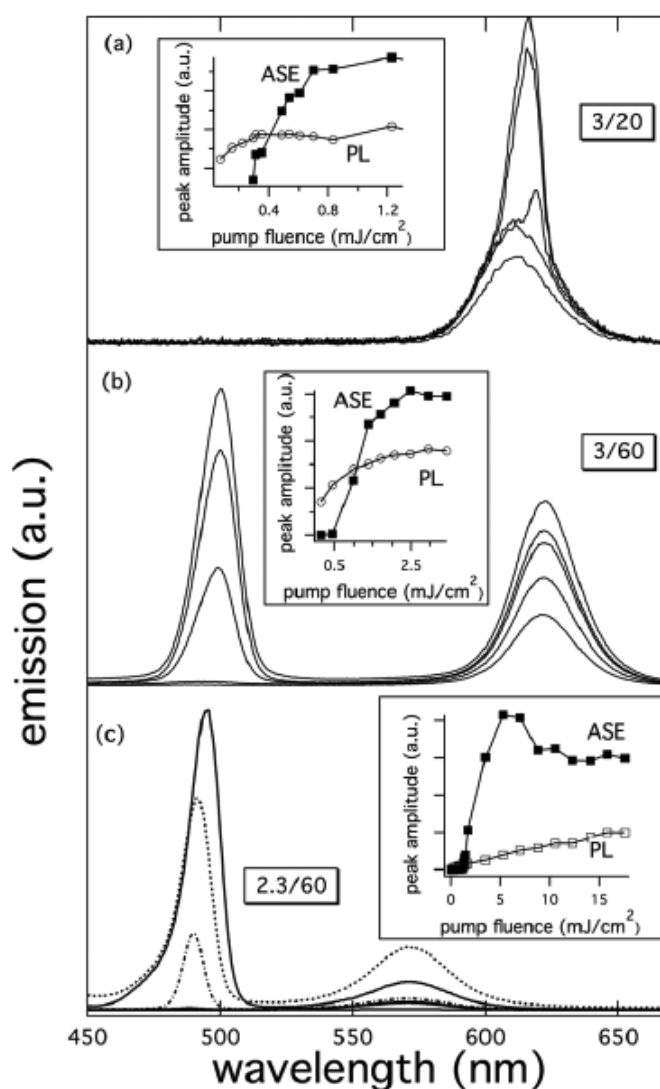
Fig. 8. Amplified spontaneous emission from a dense layers of core-shell nanorods with different core and shell size recorded at different values of pump fluence. Taken with permission from (Krhane et al., 2011a).

Then, a self-assembled oriented layer of laterally aligned nanords was transferred onto the CBP via a stamping technique. After the nanorod deposition the structure was over-coated with a 3-(4-biphenylyl)-4-phenyl-5-*t*-butylphenyl-1,2,4-triazole (TAZ) hole blocking layer (HBL), the tris(8-(hydroxyl-quinoline) aluminum (Alq3) electron transporting layer (ETL), and LiF/Al electrodes. In this type of device structure the excitation formation in the nanorod layer can occur either *via* charge trapping or *via* Forster energy transfer process from the organic material (Li et al, 2005; Anikeeva, 2007).

Amplified spontaneous emission (ASE) can be observed from dense aggregates of nanorods, for example in the form of nanorod layers fabricated by drop deposition from highly concentrated nanorod solutions onto planar surfaces. **Fig.8a** shows ASE from core states recorded from relatively short nanorods with large CdSe core. For rods with a length significantly larger than 25 nm ASE from the shell states, at 490 nm, was observed, while the photoluminescence from the core transitions was maintained, as can be seen in **Fig.8b-c**.

Lasing devices based on colloidal semiconductor nanorods have, to the best of our knowledge, only been obtained by optical pumping so far. In order to obtain lasing, an optical gain medium has to be positioned into a resonant cavity that provides sufficient feedback. Core-shell nanorods have demonstrated optical gain both from the core (Zavelani-Rossi, 2010b), and recently also from the shell emission (Krahne et al., 2011b). A conventional approach to obtain optical feedback is to embed the optical gain medium into an external resonator, for example a physical cavity consisting of a series of Bragg mirrors. However, this approach is not straightforward for self assembled layers of nanocrystals as gain medium because the roughness and thickness of this layer cannot be well controlled. An innovative solution to this problem was demonstrated by Zavelani et al. who used the nanorod layer itself as a resonant cavity. In this work ordered assemblies of nanorods were obtained via the coffee stain effect, i.e. the fluid dynamics in an evaporating droplet (Zavelani-Rossi, 2010b). Here the nanorods self assembled in large-scale ordered superstructures that are reminiscent of nematic/smectic liquid crystal phases. In particular, a dense and highly ordered region was obtained at the edge of the film that formed the outer ring (see **Fig.9a**). Within this outer ring the rods were well aligned and on average the long axis of the nanorods was oriented parallel to the ring edge. From such ordered regions of nanorods polarized emission (Carbone et al., 2007) and directionally dependent photoconductivity (Persano et al., 2010) have been observed. **Fig.9b** shows lasing spectra recorded from regions of the outer ring demonstrating that the lateral facets of the ring can function as a Fabry-Perot resonator.
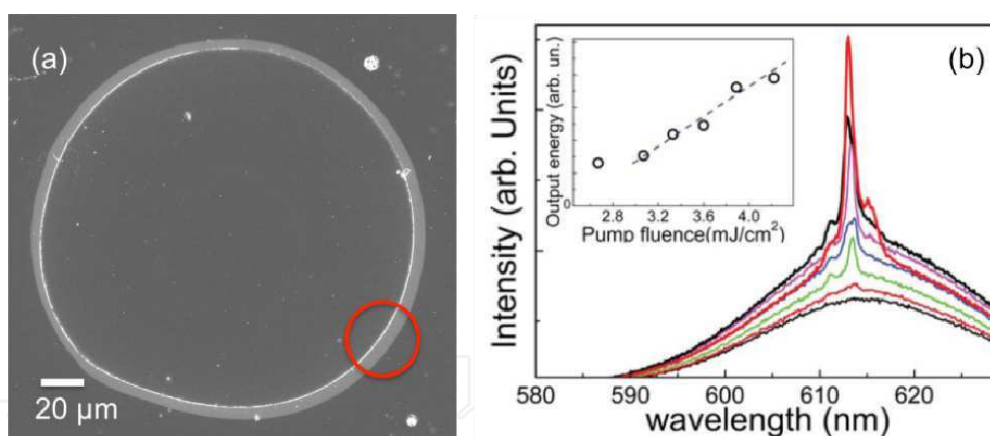

Fig. 9. Scanning electron microscopy image of a coffee stain ring that showed lasing. The red circle illustrates a spot from which lasing spectra were recorded. (b) Emission spectra above and below lasing threshold. The inset shows the characteristic input-output curve of a lasing device.

Such self-assembled micro-lasers provide new possibilities for the integration of narrow band emitters into device architectures such as lab-on-chip for point of care diagnostics, or for optical components in local area network datacom structures. Although the technology regarding light emitting devices based on colloidal nanorods is still in its infancy, the results described in this section are very encouraging and this bottom –up technology can be expected to take larger impact in the lighting industry in the near future.

4. Elongated nanoparticle arrays

The label-free ultrasensitive detection of biological molecules such as proteins, nucleic acids etc. is of utmost importance in the field of clinical medicine, especially with regards to the early diagnosis of diseases (Rosi & Mirkin, 2005). Vibrational spectroscopies (i.e. Raman Scattering and IR absorption) allow for direct detection of biological species (Colthup et al., 2010), but their cross-sections are extremely low in common experimental conditions. The possibility to excite localized surface plasmon resonances (LSPRs) in metallic nanoparticles has indicated a feasible and efficient way for enhancing the electromagnetic field on the local scale (Bohren & Huffman, 1998; Nie & Emory, 1997).

Therefore, the combination of plasmonic nanostructures with vibrational spectroscopies can be used to manipulate light-matter interactions, giving rise to fascinating perspective towards the production of novel biosensor devices (Anker et al., 2008; Das et al., 2009; De Angelis, 2008, 2010b). There is thus intensive activity oriented at the fabrication of tailored nanostructures endowed with the desired plasmonic properties. Metal nanoparticles present specific optical properties that depend on their size and geometry. While a symmetrical shape allows for polarization-independent plasmonic excitation, a dichroic absorption is expected in elongated NPs (Toma et al., 2008; Fazio et al., 2011). Beside this, the opto-plasmonic response can be additionally tailored by acting on the nanoparticle distribution and mutual coupling (Fischer & Martin, 2008).
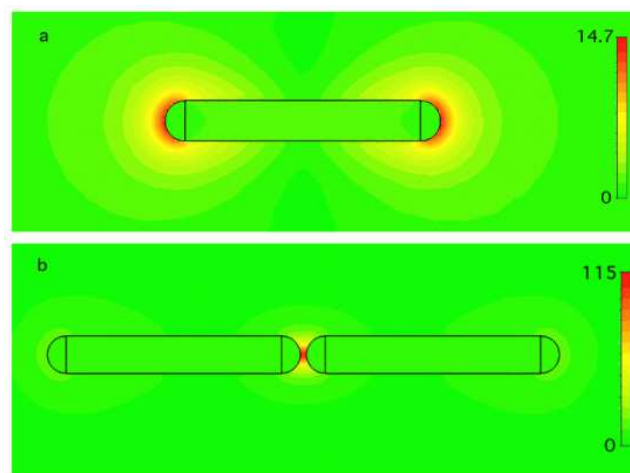

Fig. 10. (a) Calculated absolute value of the electric field distribution around an isolated nanostructure. The illuminating plane wave impinges perpendicularly on the array, and is polarized along the long axis of the elongated nanoparticle. The metallic structure length is 410 nm, while its width and height are set to 60 nm. The excitation wavelength is $\cong 1.9$ μm (b) Field distribution in the case of coupled nanostructures (gap width: 10 nm).

In order to elucidate this peculiar behavior, we have performed 3D numerical simulations using a commercial software based on a finite integration technique (CST, Computer Simulation Technology, Darmstadt, Germany). **Fig.10** shows the absolute value of the electric field around the nanostructures, on a plane that is perpendicular to the direction of the illuminating wave and cuts the nanostructure exactly at its half height. While an isolated particle concentrates the radiation at its extremities (**Fig.10a**), a dimer (i.e. a couple of closely

spaced particles) creates a "hot spot" (Fischer & Martin, 2008; Stockman et al., 1994) in correspondence of the inter-particle nanocavity (**Fig.10b**).
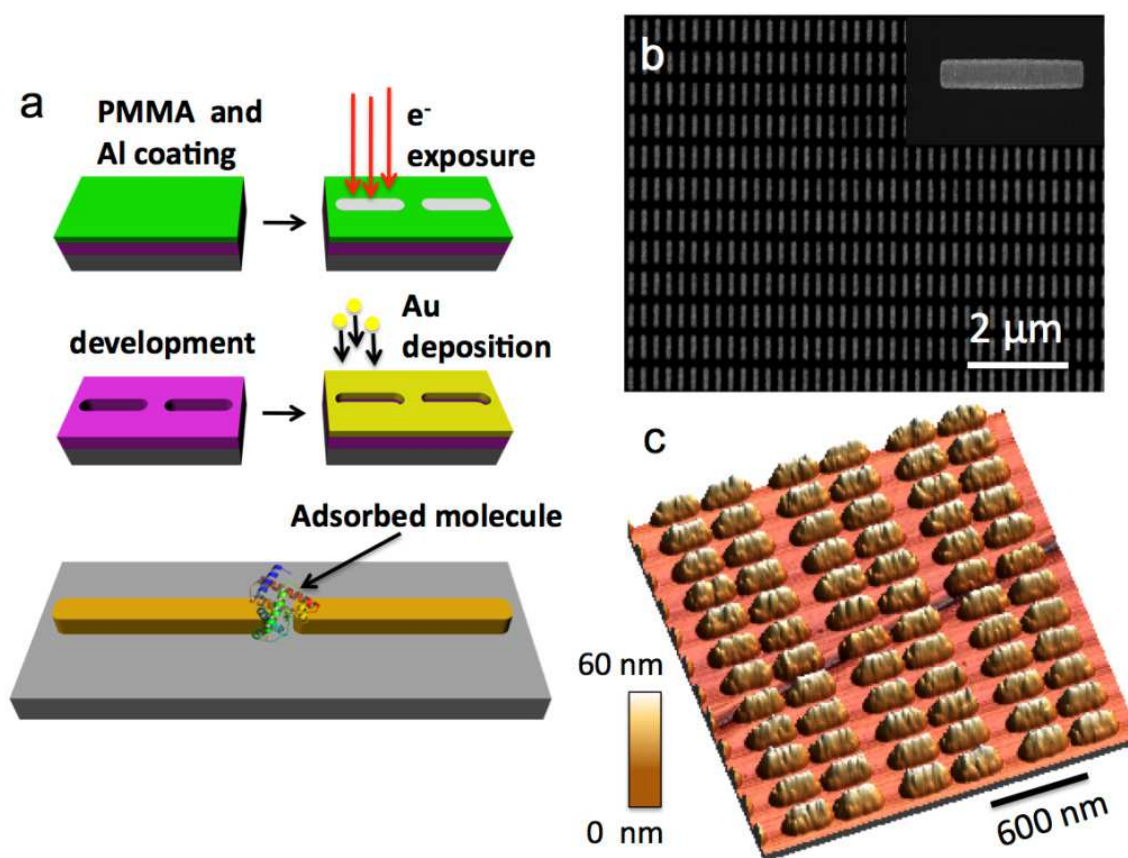

Fig. 11. (a) Schematic block diagram of the fabrication process. The last cartoon highlights the nano-biosensor concept: fabrication of a highly sensitive and specific device based on plasmonic signal enhancement. (b, c) Representative SEM and AFM images of two different nanoparticle arrays fabricated by EBL technique. The NPs are 410 nm (b) and 200 nm (c) long, while width and height are both set at 60 nm for all the structures.

Here we investigate these two specific examples, i.e. uncoupled and dimer nanoparticle arrays, with the aim to prove that their field enhancement and localization capabilities can be used for high-sensitivity Raman spectroscopy. A schematic diagram, summarized in **Fig.11a**, elucidates the main steps involved in the fabrication process. A 120 nm thick layer of PMMA (950K) was spin-coated on a CaF_2 (100) substrate. To prevent charging effects during the electron exposure, a 10 nm thick Al layer was thermally evaporated on the PMMA surface. Electron beam direct-writing of the nanoparticle patterns was carried out using a high resolution Raith150-Two e-beam writer at 15 keV beam energy and 25 pA beam current. After the Al removal in a KOH solution, the exposed resist was developed in a conventional solution of MIBK:IPA (1:3) for 30 s. Then, a 5 nm adhesion layer of Ti and a 60 nm Au film were evaporated, using a 0.3 Å/s deposition rate in a 10^{-7} mbar vacuum chamber (Kurt J Lesker PVD75). Finally, the unexposed resist was removed with acetone and rinsed out in IPA. Large scan overviews of different nanostructure arrangements are reported in Fig. 2b,c. The sample topography has been characterized recurring to scanning

electron microscopy (SEM) and atomic force microscopy (AFM, Veeco MultiMode with NanoScope V controller) equipped with ultra-sharp Si probes (ACLA-SS, AppNano) and operating in tapping mode. The resulting arrays present, as shown in **Fig.11b,c**, a high degree of reproducibility with a surface RMS roughness value of around 1 nm.

The optical properties of the nanoparticle array were investigated by means of spectroscopic transmission of polarized light in the range between 450 and 900 nm (see **Fig.12a,b**). For this purpose, we used a fiber-optic spectrometer (AvaSpec-256, Avantes) while the light source was a combined deuterium-halogen lamp (AvaLight-DHc, Avantes). The polarization of the incident light was varied from parallel to perpendicular orientation with respect to the long axis of the nanostructure. **Fig.12a** shows the results concerning isolated nanoparticles while in **Fig.12b** we report transmission spectra for coupled nanostructures. In both cases the optical transmittance spectra present evidence of a clear anisotropic behavior; for perpendicular polarization a localized minimum around 620 nm is found. This is the typical behavior exhibited by sub-wavelength metal nanoparticles sustaining a localized surface plasmon resonance (Bohren & Huffman, 1998). For parallel polarization a red shifted extinction peak, centered around 700 nm, is observed. This can be attributed to a higher order plasmonic resonance (Aizpurua et al., 2005).
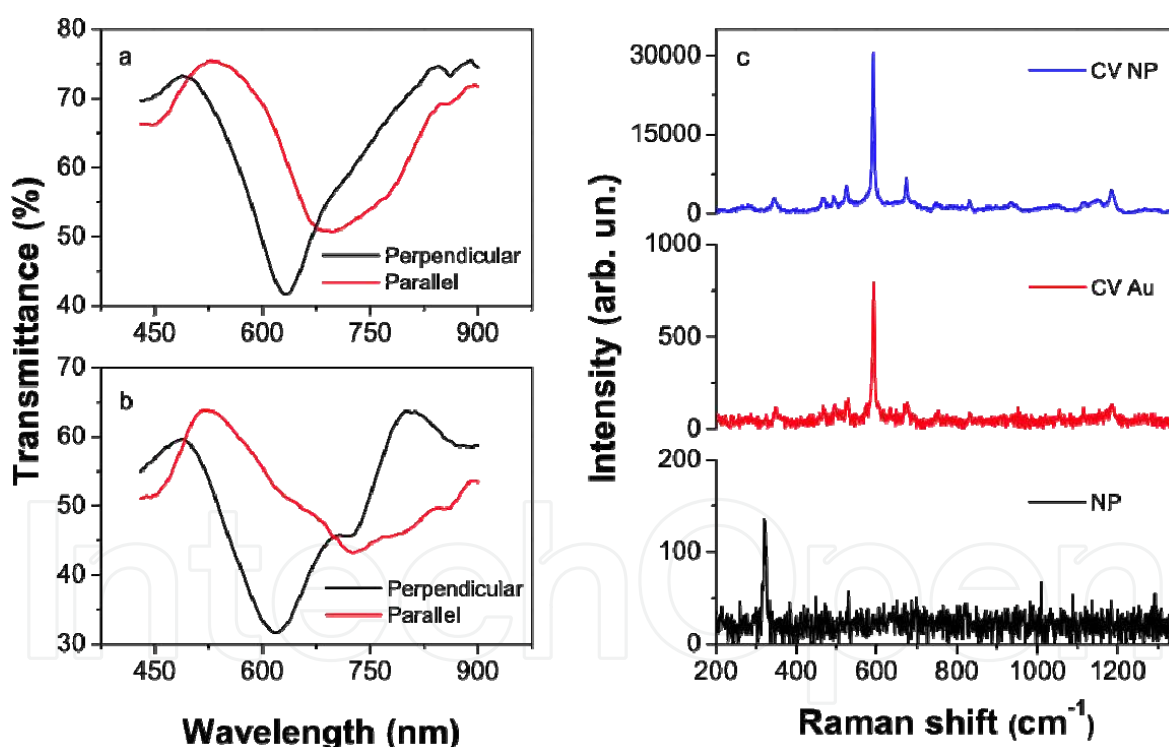

Fig. 12. Transmission optical spectra of single (a) and coupled (b) nanoparticle arrays. Red/black lines are for perpendicular and parallel polarization respectively. (c) SERS spectra of cresyl violet molecules deposited on NP sample (blue line) and flat Au film (red line). Background measurement performed on bare NP structure is also reported (black line).

Moving from the isolated nanoparticle array (**Fig.12a**) to the dimer case (**Fig.12b**) we can notice a broadening and a slightly shift of the resonance peaks due to near field coupling (Fischer & Martin, 2008).

In order to probe the enhancement behavior in Raman spectroscopy related to the plasmon excitation, the sample of **Fig.11b** was immersed in a cresyl violet (CV) solution (3.46 μ M in H_2O) for 15 min. The sample was gently rinsed in DI-water to remove molecules in excess not chemisorbed on the metal surface and then dried in nitrogen flow. SERS measurements were carried out by means of inVia microspectroscopy (Renishaw). The samples were excited by 633 nm laser wavelength (laser power = 0.14 mW and accumulation time = 50 s) through a 150X objective. The measurements were performed on bare nanoparticle arrays (sample NP), on CV molecules chemisorbed on a flat Au film (sample CV Au) and on CV deposited on the nanostructure arrays (sample CV NP). As shown in **Fig.12c** (NP line) no characteristic Raman band, except at around 320 cm^{-1} related to the Ca-F vibration from the substrate, is observed. The characteristic vibrational bands of CV are observed in the SERS spectrum (CV NP trace). Intense Raman bands centered at around 591, 882, 927 and 1189 cm^{-1} can be attributed to the N-H_2 rocking vibration, two benzene group bending, out-of phase N-H_2 rocking vibration, and combination of N-H_2 rocking and C-H_X rocking, respectively (Vogel, 2000; Sackmann et al., 2007). CV molecules chemisorbed over a flat Au film are also shown in **Fig.12c**. We can clearly observe that there is a giant enhancement in Raman signal for CV NP sample with respect to the CV Au one. The evaluated SERS enhancement for the fabricated device is around 10^7.

5. NPs based plasmonics devices for SERS applications

Metallic NPs are characterized from a great mobility of theirs electrons, resulting in a characteristic ability of sustaining coherent electronic oscillations, when light is impinged on them. The phenomenon, interesting generally the metallic surfaces, consists of the localized surface plasmons (LSP) formation (Raether, 1988; McCall et al., 1980; Haynes et al., 2005; Das et al., 2009; Kneipp et al., 2002) associated to the collective oscillation of the electrons moving in the small metal particles volume. The local electromagnetic field near the nanostructures surface results enormously enhanced. This property makes metallic NPs particularly interesting in spectroscopy. In Raman spectroscopy, this phenomenon is known as Surface Enhanced Raman Scattering (SERS) effect; it allows the detection or very diluted solutions, where very few molecules are present, overcoming the normal limit of Raman due to the great fluorescence which, in these cases, may cover molecules signals (Kneipp et al., 1997; De Angelis, 2008, 2010b). In fact, when a molecule is very close to a metallic nanostructure the LSP formation, under the laser effect, generates a giant enhancement of Raman signal (Das et al., 2009; Nie & Emory, 1997; Creighton et al., 1979).

It is clear that LSPR and, consequently, SERS intensity is strongly influenced from size, shape, inter–particle spacing of the nanoparticles and the dielectric environment of material. For particles diameters d « λ (λ = wave length of excitation laser), electrons move in phase on the excitation wave plan with the consequently formation of polarization charges and, then, of a dipolar field on particles surface. The estimated enhancement for Au and Ag isolated particles is around to 10^6 –10^7 (Otto, 1984; Kneipp & Kneipp, 2006).

For this reason the roughness of a surface obtained from a NPs deposition is of fundamental importance and overall the fabrication of specific metal nanostructures, in which size, shape, inter–particle spacing of the nanoparticles may be chosen carefully, has become an important factor for research on plasmonic devices (Gunnarsson et al., 2001). Traditionally,

as already mentioned above, NPs for SERS applications were prepared in chemical way, producing Ag colloids to whom attacking bio-molecules for the detection (Xu et al., 1999; Kneipp et al., 2004; Hao & Schatz, 2004) with good results regarding SERS effect, but with some limits in the reproducibility of the systems. Afterwards, other kinds of SERS substrates were realized, as metallic films (Constantino et al., 2002; Garoff et al., 1983) and nanostructures (NPs) with characteristic length scale in the nanometer range, as nanovoids, nanoshells, nanorods, nanorings and nanocubes (Le Ru et al., 2008; Grzelczak et al., 2010; Tao et al., 2008). Recently development of nanofabrication techniques, as electron beam lithography (EBL) or focalized ion beam (FIB), has improved plasmonic nanostructures control and consequently has improved the efficiency of these nano-devices, focalizing the attention on substrate-bound nanostructure fabrication (Zhang et al., 2006).

Here, the fabrication of silver/gold nano-aggregates into well-defined lithographic structures is described. Micro- and nano- structured patterns are realized by EBL. The procedure of fabrication consists in three steps: 1)spin-coating of the silicon wafer by a resist, ZEP for microstructures and PMMA-A2 for the nano-structures; 2)the spinned resist is exposed to high energy electrons to design the pattern; 3)the exposed resist is removed by the appropriate solvent (developer). The exposition phase is regulated by means of typical EBL parameters, as electron beam current and exposition time, regulated on the basis of resist characteristics, on its thickness and on pattern size.

The metallic nanoparticles (especially gold and silver) may be fabricated into the lithographic pattern by physical techniques (evaporation), chemical techniques (reduction from metallic ions) or self-assembly techniques (Jensen et al., 1999; Felidj et al., 2002).

Among these, electroless deposition is a very fast, simple and economic technique, based on the auto-catalytic reduction of metal salts. The redox reaction consists in an electrons exchange between the metallic ions of an opportune solution where the substrate is immersed, and a reducing agent, which may be in the same solution or may be the substrate itself. In literature, several studies report the deposition of metals, as silver, gold, copper, nickel or their alloy, by this technique, obtaining thin films with higher roughness, dendritic structures, submicrometric metallic structures or NPs (Qiu & Chu, 2008; Gao et al., 2005; Yang et al., 2008; Peng & Zhu, 2004; Goia & Matijevic, 1998).

Here, the attention is centered on deposition of silver and gold nanoparticles for SERS application by electroless technique in which the reducing agent is the substrate itself (Coluccio et al., 2009). After the resist developing (the 3° steps of lithographic process) the pattern on Si wafer consists in holes where silicon remains uncovered. The patterned substrate is then dept into a solution of silver nitrate ($AgNO3$) or chloroauric acid ($HAuCl_4$) prepared in fluoridric acid. The standard solution concentration is around 1 mM, but it is possible to modulate it according to the morphology that we want to obtain. The solution enters the cavity and the reaction between silver/gold ions and the silicon wafer occurs. The metal deposition increases with the increase of temperature and reaction time.

The electroless process may be divided in two steps:

1. the patterned silicon reacts with fluoridric acid (HF) determines the removing of the superficial silicon oxide (SiO_2) layer and the formation of a hydrogenated surface, inert
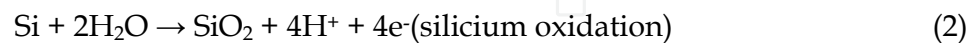
to reactions with O_2, CO_2, CO, etc., while presenting a good reactivity with silver ions (Palermo & Jones, 2001);

2. the metal nano grains growth into the holes obtained onto the substrate, according the following reactions:
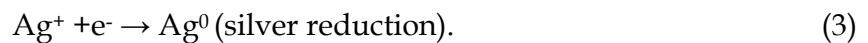
$$4\ Ag^+ + Si(s) + 6\ HF \rightarrow 4Ag^0 + H_2SiF_6 + 4H^+ \tag{1}$$

which can be separated into two half-cell reactions (2) and (3):

Anode

$$Si + 2H_2O \rightarrow SiO_2 + 4H^+ + 4e^-\text{(silicium oxidation)} \tag{2}$$

Cathode

$$Ag^+ + e^- \rightarrow Ag^0\text{ (silver reduction).} \tag{3}$$

The oxidation of silicon, produced the electrons, is necessary for the silver reduction (Goia & Matijevic, 1998; Coluccio et al., 2009; Palermo & Jones, 2001). The mechanism of formation of the nanoparticles begins with few silver ions that react directly with the substrate forming metallic nuclei. These Ag nuclei are strongly electronegative, thereby, attracting other electrons from the silicon bulk and consequently getting negatively charged; then they attract silver ions which reduced to Ag^0 thus inducing the growth of the original Ag nuclei (Qiu & Chu, 2008). The gold reactions are very similar, the ion reacting obviously is Au^{3+}. Gold forms smaller NPs then silver and the reaction kinetic is slower.

The morphology of nano-aggregates depends on the lithographic pattern and, in particular, on the size: in nano sized structures, the grains grow compact and more mild reaction conditions are necessary for avoiding an excessive nano grains formation, in particular, concentrations under 1 mM and temperatures under 50°C may be used. In micro sized structures, for obtaining a uniform surface covering is important to use concentration up to 1mM and temperature around 50°C. For every SERS structures, the optimal reaction conditions must be searched, modulating the parameter for obtaining the correct particles sizes and density.

Both gold and silver nano aggregates give a good SERS effect, even if silver has the disadvantage that oxidizes with time, giving a decreasing of SERS efficiency. To overcome this problem bimetallic substrates may be fabricated depositing in a first step silver nano grains and over them gold nano grains. Gold assures the SERS device protection from time depending oxidation and maintains a good efficiency of the substrate. SEM images of silver and gold SERS devices are shown in **Fig.13**.

As mentioned above the fabrication of regular array of metallic NPs, may increase the efficiency and the reproducibility of the SERS device, and their optical characteristics may be selected varying size and mutual distance between particles. NPs arrays examples are reported in **Fig.14**.
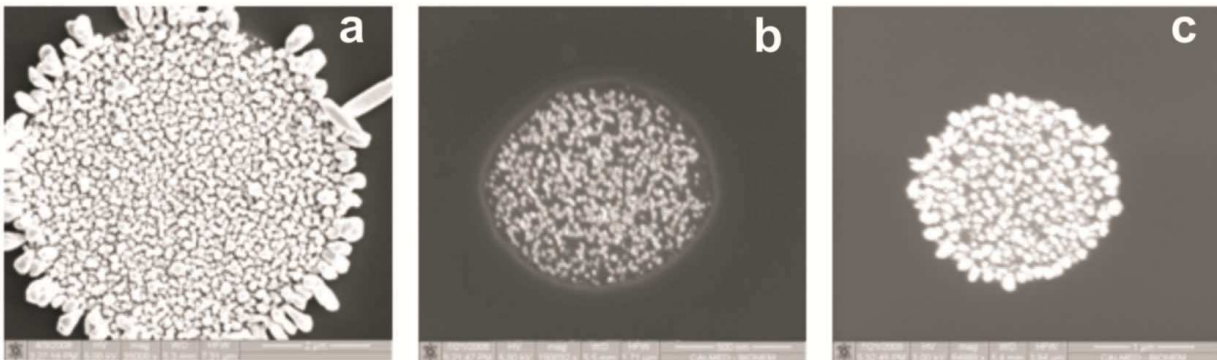
Fig. 13. SEM images of nano grains assembled on microstructures, fabricated using e-beam lithography and electroless deposition: (a) silver nano grains, (b) gold nano grains, (c) silver/gold nano grains.
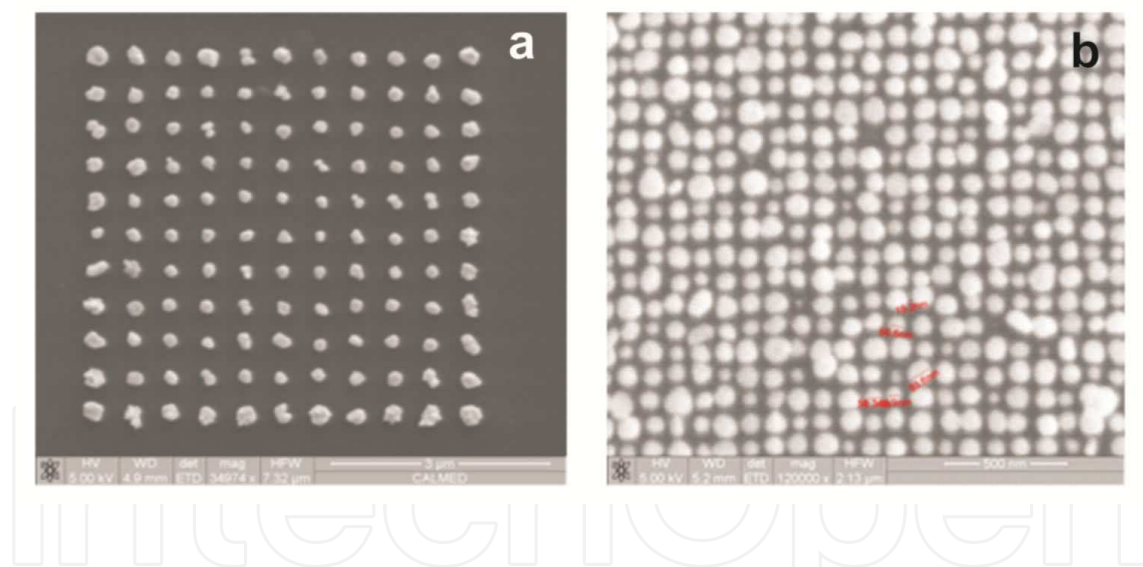

Fig. 14. SEM images of nano grains assembled on nanostructures, fabricated using e-beam lithography and electroless deposition.

The SERS effect of gold, silver or of bimetallic (silver/gold) microstructures is investigated using rhodamine-6G as probe molecules. The substrates are dipped into rhodamine-6G water solution with different concentrations, rinsed with water dried in N_2 and then used for the spectroscopic investigation. SERS experiments show spectra with well-defined peaks at very low molecular concentration, for all the metallic/bimetallic substrates (**Fig.15**). The highest SERS efficiency is found for SERS device based on gold over silver surface.
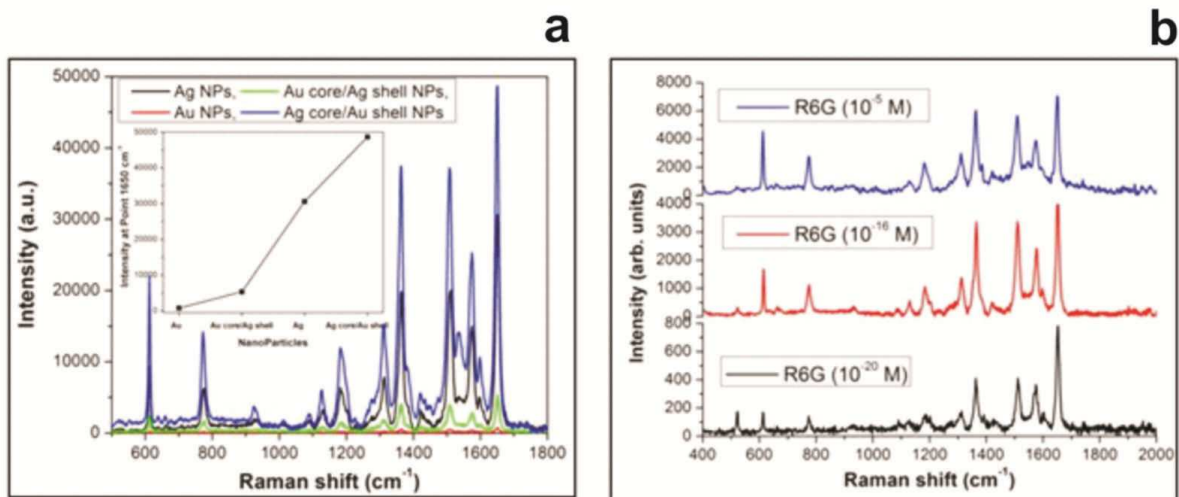
Fig. 15. a) R6G [10⁻¹²M], absorbed on the silver, gold, Ag/Au and Au/Ag structures. Raman signal increases from Au, Au core/Ag shell, Ag and Ag core/Au shell; b) 3. SERS spectra acquired from 10⁻⁵, 10⁻¹⁶ and 10⁻²⁰ M R6G, absorbed on the silver nanostructures.

6. References

Aizpurua, J.; Bryant, G. W.; Richter, L. J.; Garcia de Abajo, F. J.; Kelley, B. K. & Mallouk, T. (2005). Optical properties of coupled metallic nanorods for field-enhanced spectroscopy. *Phys. Rev. B,* Vol. 71, pp. 235420.

Anikeeva, P.O., et al., Electroluminescence from a mixed red-green-blue colloidal quantum dot monolayer. Nano Letters, 2007. 7(8): p. 2196-2200.

Anker, J. N.; Hall, W. P.; Lyandres, O.; Shah, N. C.; Zhao, J. & Van Duyne, R. P. (2008). Biosensing with plasmonic nanosensors. *Nature Materials,* Vol. 7, pp. 442-453.

Bohren, C. F. & Huffman, D. R., (1998). *Absorption and Scattering of light by small particles* (Wiley, New York).

Canham L., Properties of Porous Silicon. INSPEC - The Institution of Electrical Engineers London - United Kingdom, 1997.

Carbone, L., et al., Synthesis and micrometer-scale assembly of colloidal CdSe/CdS nanorods prepared by a seeded growth approach. Nano Letters, 2007. 7(10): p. 2942-2950.

Cohen M. H., Melnik K., Boiasrki A., Ferrari M. & Martin F. J., Microfabrication of silicon-based nanoporous particulates for medical applications, *Biomed. Microdevices* (5), 253–259, 2003.

Colthup, N. B., Daly, L. H. & Wiberley, S. E., (2010). *Introduction to Infrared and Raman Spectroscopy* (Academic Press, USA).

Coluccio M.L., Das G., Mecarini F., Gentile F., Pujia A., Bava L., Tallerico R., Candeloro P., Liberale C., De Angelis F., Di Fabrizio E., Silver-based surface enhanced Raman scattering (SERS) substrate fabrication using nanolithography and site selective electroless deposition, Microelectronic Engineering 86 (2009) 1085–1088.

Constantino C.J.L., Lemma T., Antunes P.A., Aroca R., Single molecular detection of a perylene dye dispersed in a Langmuir–Blodgett fatty acid monolayer using surface-

enhanced resonance Raman scattering, Spectro chimica Acta Part A 58 (2002) 403–409.

Creighton J. A., Blatchford C. G., Albrecht M. G., Plasma Resonance Enhancement of Raman-Scattering by Pyridine Adsorbed on Silver or Gold Sol Particles of Size Comparable to the Excitation Wavelength, J. Chem. Soc., Faraday Trans II 75 (1979) 790-798.

Crommelin D.J.A., Schreier H., Liposomes, in: *Colloidal Drug Delivery Systems*, J. Kreuter, editor. Marcel Dekker, Inc. New York, 1994.

Das G., Mecarini F., Gentile F., De Angelis F., Kumar M., Candeloro P., Liberale C., Cuda G., Di Fabrizio E., Nano-patterned SERS substrate: Application for proteinanalysis vs. temperature, Biosens. Bioelectron. 24 (2009) 1693–1699.

De Angelis, F.; Patrini, M.; Das, G.; Maksymov, I.; Galli, M.; Businaro, L.; Andreani, L. C. & Di Fabrizio, E. (2008). A Hybrid Plasmonic Photonic Nanodevice for Label-Free Detection of a Few Molecules. *Nano Letters*, Vol. 8, No. 8, pp. 2321–2327

De Angelis F., Pujia A., Falcone C., Iaccino E., Palmieri C., Liberale C., Mecarini F., Candeloro P., Luberto L., de Laurentiis A., Das G., Scala G., and Di Fabrizio E., Water soluble nanoporous nanoparticles for in vivo targeted drug delivery and controlled release in b cells tumor context. Nanoscale, 2:2230-2236, 2010.

De Angelis, F.; Das, G.; Candeloro, P.; Patrini, M.; Galli, M.; Bek. A.; Lazzarino, M.; Maksymov, I.; Liberale, C.; Andreani, L. C. & Di Fabrizio, E. (2010). Nanoscale chemical mapping using three-dimensional adiabatic compression of surface plasmon polaritons. *Nature Nanotech.*, Vol. 5, pp. 67-72

Decuzzi P. and Ferrari M., The Adhesive Strength of Non-Spherical Particles Mediated by Specific Interactions, *Biomaterials*, 27(30):5307-1534, 2006.

Decuzzi P., Causa F., Ferrari M. and Netti P. A., The Effective Dispersion of Nanovectors Within the Tumor Microvasculature, *Ann Biomed Eng.*, 34(4):633-641, 2006.

Decuzzi P. and Ferrari M., The Role of Specific and Non-Specific Interactions in Receptor-Mediated Endocytosis of Nanoparticles, *Biomaterials*, 28(18):2915-2922, 2007.

Duncan R., The dawning era of polymer therapeutics, *Nature Rev. Drug Discov.* (2), 347–360, 2003.

Fazio B.; D'Andrea, C.; Bonaccorso, F.; Irrera, A.; Calogero, G.; Vasi, C.; Gucciardi, P. G.; Allegrini, M.; Toma, A.; Chiappe, D.; Martella, C. & Buatier De Mongeot F. (2011). Re-radiation Enhancement in Polarized Surface-Enhanced Resonant Raman Scattering of Randomly Oriented Molecules on Self-Organized Gold Nanowires. *ACS Nano*, Vol. 5 No. 7, pp. 5945-5956.

Felidj N., Aubard J., Levi G., Krenn J.R., Salerno, Schider G., Lamprecht B., Leitner A., Aussenegg F.R., Controlling the optical response of regular arrays of gold particles for surface enhanced Raman scattering, Phys. Rev. B Condens. Matter Mater. Phys. 65 (2002) 075419/1–075419/9.

Ferrari M., Cancer Nanotechnology: opportunities and challenges, *Nature Reviews Cancer*, 2005; (5):161-171.

Fischer, H. & Martin, O. J. F. (2008). Engineering the optical response of plasmonic nanoantennas. *Optics Express,* Vol. 16 No.12, pp. 9144-9154.

Gao J., Tang F., Ren J., Electroless nickel deposition on amino-functionalized silica spheres, Surface & Coatings Technology 200 (2005) 2249–2252.

Garoff S., Weitz D.A., Alvarez M.S. and Chung J.C., Electromagnetically Induced Changes in Intensities, Spectra and Temporal Behavior of Light Scattering from Molecules on Silver Island Films, J. Phys. Colloq. 44, C10 (1983) 345-348.

Gentile F., Ferrari M., Decuzzi P. (2007), Transient Diffusion of Nanovectors in Permeable Capillaries, J. Serbian Soc. Comput. Mech., 1(1), 1-19.

Gentile F., Ferrari M. and Decuzzi P., `The Transport of Nanoparticles in Blood Vessels: The Effect of Vessel Permeability and Blood Rheology`, Annals of Biomedical Engineering, 2008:2(36); 254–261.

Gilles E. M. & Frechet J. M. J., Designing macromolecules for therapeutic applications: Polyester dendrimerpolyethylene oxide 'bow-tie' hybrids with tunable molecular weights and architecture, J. Am. Chem. Soc. (124), 14137–14146, 2002.

Godefroo S., Hayne M., Jivanescu M., Stesmans A., Zacharias M., Lebedev O.I., van Tendeloo G., and Moschchalkov V. V., Classification and control of the origin of photoluminescence from si nanocrystals. Nature Nanotechnology, 3:174-178, 2008.

Granitzer P. and Rumpf K., Porous silicon - a versatile host material. Materials, 3:943-998, 2010.

Grzelczak M., Vermant J., Furst E. M., Liz-Marza´n L. M., Directed Self-Assembly of Nanoparticles, ACSNano VOL. 4 ▪ NO. 7 ▪ 3591–3605 ▪ 2010;

Gunnarsson L., Bjerneld E.J., Xu H., Petronis S., Kasemo B. and Käll M., Interparticle-coupling effects in Nanofabricated Substrates for Surface Enhanced Raman Scattering, Applied Physics Letters 78, 802-804 (2001).

Halimaoui A., Porous silicon: material processing, properties and applications, in JC Vial and J. Derrien (editors), Porous silicon science and technology, Springer-Verlag (1995).

Hao E. and Schatz G. C., Electromagnetic fields around silver nanoparticles and dimmers, J. Chem. Phys. 120 (2004) 357-367.

Haynes C.L., McFarland A.D., VanDuyne R.P., Surface-Enhanced Raman Spectroscopy, Anal. Chem. 77 (2005) 338A-346A.

Hirsch, L. R., Halas, N. J. & West, J. L. Nanoshell-mediated near-infrared thermal therapy of tumors under magnetic resonance guidance, Proc. Natl Acad. Sci. USA (100), 13549–13554, 2003.

Hu, J.T., et al., Linearly polarized emission from colloidal semiconductor quantum rods. Science, 2001. 292(5524): p. 2060-2063.

Jensen T.R., Schatz G.C., Van Duyne R.P., Nanosphere Lithography: Surface plasmon resonance spectrum of a periodic array of silver nanoparticles by UV-vis extinction spectroscopy and electrodynamic modeling, J. Phys. Chem. B 103 (1999) 2394–2401 .

Jeyarama S. Ananta, Biana Godin, Richa Sethi, Loick Moriggi, Xuewu Liu, Rita E. Serda, Ramkumar Krishnamurthy, Raja Muthupillai, Robert D. Bolskar, Lothar Helm, Mauro Ferrari, Lon J. Wilson, Paolo Decuzzi, Geometrical confinement of gadolinium-based contrast agents in nanoporous particles enhances T_1 contrast, Nature Nanotechnology 5, 815–821 (2010).

Ji-Ho Park, Luo Gu, Geo rey von Maltzahn, Erkki Ruoslahti, Sangeeta N. Bhatia, and Michael J. Sailor. Biodegradable luminescent porous silicon nanoparticles for in vivo applications. Nature Materials, 8:331, 336, 2009.

Kazes, M., et al., Lasing from semiconductor quantum rods in a cylindrical microcavity. Advanced Materials, 2002. 14(4): p. 317-321.

Kazes, M., et al., Lasing from CdSe/ZnS quantum rods in a cylindrical microcavity. Quantum Dots, Nanoparticles and Nanowires, 2004. 789: p. 11-16429.

Kircher M. F., Mahmood U., King, R. S., Weissleder R. & Josephson L., A multimodal nanoparticle for preoperative magnetic resonance imaging and intraoperative optical brain tumor delineation, *Cancer Res.* (63), 8122–8125, 2003.

Klibanov A. L. et al., Activity of amphipathic PEG 5000 toprolong the circulation time of liposomes depends on the liposome size and is unfavourable for immunoliposome binding to target, *Biochem. Biophys. Acta* (1062), 142–148, 1991.

Kneipp K., Wang Y., Kneipp H., Perelman L.T., Itzkan I., Dasari R. R., and Feld M. S., Single Molecule Detection using Surface-Enhanced Raman Scattering, Phys. Rev. Lett. 78 (1997) 1667-1670.

Kneipp K., Kneipp H., Itzkan I., Dasari R. R., Feld M.S., Kneipp H., Itzkan I., Dasari R. R., and Feld M. S., Surface-enhanced Raman scattering and biophysics, J. Phys. Condens. Matter 14 (2002) R597-R624.

Kneipp, K., Kneipp, H., Abdali, S. et al., Single Molecule Raman Detection of Enkephalin on Silver Colloidal Particles. Spectroscopy 18 (2004) 433–440.

Kneipp K., Kneipp H., Kneipp J., Surface-Enhanced Raman Scattering in Local Optical Fields of Silver and Gold Nanoaggregatess From Single-Molecule Raman Spectroscopy to Ultrasensitive Probing in Live Cells, Acc. Chem. Res. 39 (2006) 443-450.

Krahne, R., et al., Amplified Spontaneous Emission from Core and Shell Transitions in CdSe/CdS Nanorods fabricated by Seeded Growth. Applied Physics Letters, 2011. 98(6): p. 063105.

Krahne, R., et al., Physical properties of elongated inorganic nanoparticles. Physics Reports, 2011. 501(3-5): p. 75-221.

La Van D. A., McGuire T. & Langer R., Small-scale systems for *in vivo* drug delivery, *Nature Biotechnol.*, (21), 1184–1191, 2003.

Langer R., Drug delivery and targeting, *Nature* (392), 5–10, 1998.

Le Ru E.C., Etchegoin P.G., Grand J., Félidj N., Aubard J., Lévi G., Hohenau A., Krenn J.R., Surface enhanced Raman spectroscopy on nanolithography-prepared substrates, Current Applied Physics 8 (2008) 467–470.

Li, Y.Q., et al., White organic light-emitting devices with CdSe/ZnS quantum dots as a red emitter. Journal Of Applied Physics, 2005. 97(11): p. art. n. 113501.

Lupo, M.G., et al., Ultrafast Electron-Hole Dynamics in Core/Shell CdSe/CdS Dot/Rod Nanocrystals. Nano Letters, 2008. 8(12): p. 4582-4587.

McCall S.L., Platzman P.M., Wolf P.A., Surface enhanced Raman scattering, Phys. Lett. 77A (1980) 381-383.

Mitragotri Samir and Lahan Joerg, Physical approaches to biomaterial design. Nature Materials, 8:15-23, 2009.

Nie S. and Emory S. R., Probing Single Molecules and Single Nanoparticles by Surface-Enhanced Raman Scattering, Science 275 (1997) 1102-1106.

Nobile, C., et al., Self-assembly of highly fluorescent semiconductor nanorods into large scale smectic liquid crystal structures by coffee stain evaporation dynamics. Journal Of Physics-Condensed Matter, 2009. 21(26): p. 264013.

O Farrel N., Houlton A., B. R. Horrocks, Silicon nanoparticle application in cell biology and medicine. International Journal of Nanomedicine, 1(4):451-472, 2006.

Otto A., In Light scattering in solids IV. Electronic scattering, spin effects, SERS and morphic effects; M. Cardona, G. Guntherodt, Eds.; Springer-Verlag: Berlin, Germany, 1984; Vol. 1984, pp 289- 418.

Palermo, D. Jones, Morphological changes of the Si [100] surface after treatment with concentrated and diluted HF, Materials Science in Semiconductor Processing, 4 (2001) 437–441.

Park J. W., Liposome-based drug delivery in breast cancer treatment, *Breast Cancer Res.* (4), 95–99, 2002.

Peng K., Zhu J., Morphological selection of electroless metal deposits on silicon in aqueous fluoride solution, ElectrochimicaActa 49 (2004) 2563–2568.

Persano, A., et al., Photoconduction Properties in Aligned Assemblies of Colloidal CdSe/CdS Nanorods. Acs Nano, 2010. 4(3): p. 1646-1652.

Petros Robby A. and DeSimone Joseph M., Strategies in the design of nanoparticles for therapeutic applications. Nature Reviews Drug Discovery, 9:615-627, 2010.

Pujia A., De Angelis F., Scumaci D., Gaspari M., Liberale C., Candeloro P., Cuda G., Di Fabrizio E., Highly efficient human serum filtration with water-soluble nanoparticles. International Journal of Nanomedicine, 5:1005-1015, 2010.

Qiu T., Chu P.K., Self-selective electroless plating: An approach for fabrication of functional 1D nanomaterials, Mater. Sci. Eng. R 61 (2008) 59-77.

Raether H., Surface Plasmonson Smooth and Rough Surfaces and on Gratings (Springer, Berlin, 1988).

Rizzo, A., et al., Polarized Light Emitting Diode by Long-Range Nanorod Self-Assembling on a Water Surface. Acs Nano, 2009. 3(6): p. 1506-1512.

Rosi, N. L. & Mirkin, C. A., (2005). Nanostructures in Biodiagnostics. *Chem. Rev.*, Vol. 105, pp. 1547-1562.

Sackmann, M.; Bom, S.; Balster, T. & Materny, A. (2007). Nanostructured gold surfaces as reproducible substrates for surface-enhanced Raman spectroscopy. *J. Raman Spect.*, Vol. 38, pp. 277-282.

Schellenberger E. A. et al., Annexin V-CLIO: a nanoparticle for detecting apoptosis by MRI, *Mol. Imaging* (1), 102–107, 2002.

Siti M. Janib, Ara S. Moses, and J. Andrew MacKay. Imaging and drug delivery using theranostic nanoparticles. Advanced Drug Delivery Reviews, 62:1052-1063, 2010.

Stockman, M. I.; Pandey, L. N.; Muratov, L. S. & George, T. F. (1994). Giant fluctuations of local optical fields in fractal clusters. *Phys. Rev. Lett.*, Vol. 72, pp. 2486-2489.

Talapin, D.V., et al., Highly emissive colloidal CdSe/CdS heterostructures of mixed dimensionality. Nano Letters, 2003. 3(12): p. 1677-1681.

Tao A. R., Habas S., Yang P., Shape Control of Colloidal Metal Nanocrystals , Small 4 No 3 (2008), 310 – 325.

Tasciotti E, Liu X, Bhavane R, Plant K, Leonard AD, Price BK, Cheng MM, Decuzzi P, Tour JM, Robertson F, Ferrari M. Mesoporous silicon particles as a multistage delivery system for imaging and therapeutic applications, Nature Nanotechnol. 2008 3(3):151-157.

Toma, A.; Chiappe, D.; Massabò, D.; Boragno, C. & Buatier de Mongeot, F. (2008). Self-organized metal nanowire arrays with tunable optical anisotropy. *Appl. Phys. Lett.*, Vol. 93, pp. 163104.

V. Dan G., Matijevic E., Preparation of monodispersed metal particles, New J. Chem. 22 (1998) 1203–1215.

Vogel, E.; Gbureck, A. & Kiefer, W. (2000). Vibrational spectroscopic studies on the dyes cresyl violet and coumarin 152*, *J. Mol. Struct.*, Vol. 550, pp. 177-190.

Whitesides G. M., The 'right' size in nanotechnology, *Nature Biotechnol.*, (21), 1161–1165, 2003.

Xu H., Bjerneld E.J., Kall M., et al..Spectroscopy of Single Hemoglobin Molecules by Surface Enhanced Raman Scattering. Phys. Rev. Lett. 83 (1999) 4357–4360.

Yang Y., Shi J., Kawamura G., Nogami M., Preparation of Au-Ag, Ag-Au core-shell bimetallic nanoparticles for surface-enhanced Raman scattering, Scr. Mater. 58 (2008) 862-865.

Zavelani-Rossi, M., et al., Lasing in self-assembled microcavities of CdSe/CdS core/shell colloidal quantum rods. Nanoscale, 2010. 2(6): p. 931-935.

Zavelani-Rossi, M., et al., Suppression of Biexciton Auger Recombination in CdSe/CdS Dot/Rods: Role of the Electronic Structure in the Carrier Dynamics. Nano Letters, 2010. 10(8): p. 3142-3150.

Zhang Y. & Shang M., Self-assembled coatings on individual monodisperse magnetite nanoparticles for efficient intracellular uptake, *Biomed. Microdevices* (6), 33–40, 2004.

Zhang, X., Yonzon, C.R., Duyne, R.P.V. 2006. Nanosphere Lithography Fabricated Plasmonic Materials and Their Applications. *J. Mater. Res.* 21: 1083–1092.
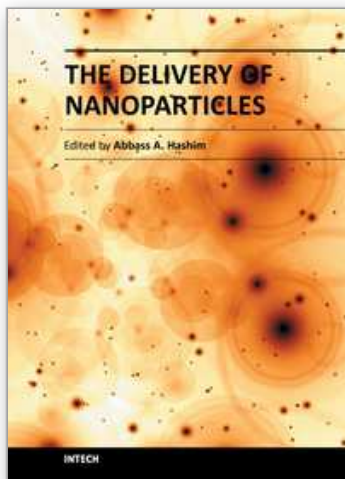
The Delivery of Nanoparticles

Edited by Dr. Abbass A. Hashim

Nanoparticle is a general challenge for today's technology and the near future observations of science. Nanoparticles cover mostly all types of sciences and manufacturing technologies. The properties of this particle are flying over today scientific barriers and have passed the limitations of conventional sciences. This is the reason why nanoparticles have been evaluated for the use in many fields. InTech publisher and the contributing authors of this book in nanoparticles are all overconfident to invite all scientists to read this new book. The book's potential was held until it was approached by the art of exploring the most advanced research in the field of nano-scale particles, preparation techniques and the way of reaching their destination. 25 reputable chapters were framed in this book and there were alienated into four altered sections; Toxic Nanoparticles, Drug Nanoparticles, Biological Activities and Nano-Technology.

How to reference

In order to correctly reference this scholarly work, feel free to copy and paste the following:

Enzo Di Fabrizio, Francesco Gentile, Michela Perrone Donnorso, Manohar Chirumamilla Chowdary, Ermanno Miele, Maria Laura Coluccio, Rosanna La Rocca, Rosaria Brescia, Roman Krahne, Gobind Das, Francesco De Angelis, Carlo Liberale, Andrea Toma, Luca Razzari, Liberato Manna and Remo Proietti Zaccaria (2012). Nanoparticles and Nanostructures for Biophotonic Applications, The Delivery of Nanoparticles, Dr. Abbass A. Hashim (Ed.), ISBN: 978-953-51-0615-9, InTech, Available from: http://www.intechopen.com/books/the-delivery-of-nanoparticles/nanoparticles-and-nanostructures-for-biophotonic-applications

INTECH
open science | open minds